Atmos. Chem. Phys. Discuss., https://doi.org/10.5194/acp-2018-1127
Manuscript under review for journal Atmos. Chem. Phys.
Discussion started: 19 November 2018
© Author(s) 2018. CC BY 4.0 License.

Atmospheric Chemistry and Physics Discussions

Arctic sea ice, Eurasia teleconnection pattern and summer surface ozone pollution in North China

Zhicong Yin [12*], Huijun Wang[12], Yuyan Li[1], Xiaohui Ma[3], Xinyu Zhang[1]

[1]Key Laboratory of Meteorological Disaster, Ministry of Education / Joint International Research Laboratory of Climate and Environment Change (ILCEC) / Collaborative Innovation Center on Forecast and Evaluation of Meteorological Disasters (CIC-FEMD), Nanjing University of Information Science & Technology, Nanjing 210044, China
[2]Nansen-Zhu International Research Center, Institute of Atmospheric Physics, Chinese Academy of Sciences, Beijing, China
[3]Institute of Urban Meteorology, CMA / Environmental Meteorology Forecast Center of Beijing-Tianjin-Hebei

**Corresponding author:* Zhicong Yin（yinzhc@163.com）

Abstract. Summer surface O_3 pollution has rapidly intensified recently, damaging human and ecosystem health. In 2017, the summer mean maximum daily average 8 h concentration of ozone was greater than 150 μg/m³ in North China. Here, we show that in addition to anthropogenic emissions, the Eurasia teleconnection pattern (EUTP), a major globally significant atmospheric teleconnection pattern, influences surface O_3 pollution in North China. The local meteorological conditions associated with the EUTP positive phase supported intense and efficient photochemical reactions to produce more surface O_3. The associated southerlies over North China transported surrounding O_3 precursors to superpose local emissions. Solar radiation and high temperature dramatically enhanced O_3 photochemical reactions. Furthermore, due to the close connection between the preceding May Arctic sea ice and summer EUTP, approximately 60% of the interannual variability of summer surface O_3 pollution was attributed to Arctic sea ice to the north of Eurasia. This finding aids in the seasonal prediction of O_3 pollution.

Keywords: ozone pollution, photochemical reaction, Eurasia teleconnection pattern, climate change, Arctic sea ice

1 Introduction

Along with social and economic development, air pollution has been increasing in China (Chen, 2013; Watts et al., 2018). The major air pollution types in China are haze pollution in winter (Yin et al., 2015; Wang, 2018) and surface ozone (O_3) pollution in summer (Ma et al., 2016; Tang et al., 2018). Due to the low visibility it caused and its obvious unusual smell, haze pollution easily causes warning and are being controlled in recent years (The environmental statistics unit of stat-center in Perking University, 2018). However, surface O_3 pollution has always occurred on clear and sunny days (Wang et al., 2017), so it is not visible to humans. The features and causes of O_3 pollution in China, especially the impacts of climate variability, have not been sufficiently studied. Europe has benefitted from its rigorous air protection act and maintained good air quality, but the surface ozone levels still showed significant increases during 1995–2012 (Yan et al., 2017). In the major urban areas in China, the surface O_3 concentrations have exceeded the ambient air quality standard by 100–200% (Wang et al., 2017), especially in the

© Author(s) 2018. CC BY 4.0 License.

Yangtze River Delta (Tong et al., 2017) and Beijing-Tianjin-Hebei region in North China (Wang et al., 2006; Shi et al., 2015).

There is rarely a direct discharge of surface O_3. The precursors of O_3 (e.g. NOx and VOC) photochemically react to generate O_3 under suitable weather conditions (An et al., 2009). Sedimentation, dynamic transport and attenuation of O_3 are closely related to atmospheric circulation. The North Atlantic Oscillation intercontinentally affects surface O_3 concentrations over Europe (Christoudias et al., 2012; Pausata et al., 2012). The summer surface O_3 variability in North America is significantly modulated by the position of the jet stream (Barnes and Fiore, 2013; Lin et al., 2015). A strong positive correlation between the East Asian summer monsoon and summer mean ozone existed during 1986–2006, based on numerical model results (Yang et al., 2014). A significantly strong west Pacific subtropical high resulted in higher relative humidity, more clouds, more rainfall, less ultraviolet radiation and lower air temperatures, which were unfavorable for the formation of O_3 (Zhao and Wang, 2017). In 2013, a severe heat wave contributed to the high O_3 concentration in the Yangtze River Delta (Pu et al., 2017). The frequency of large-scale, extreme heat events is closely related to atmospheric patterns, such as the Eurasia teleconnection pattern (EUTP; Pu et al., 2017; Li and Sun, 2018) and aerosol effective radiative forcing (Liu and Liao, 2017). The winds from a polluted area also transport O_3 and its precursors downwind (Doherty et al., 2013). Due to the close relationship between surface O_3 and meteorological conditions, the impacts of climate change on O_3 have been projected by various numerical models (Doherty et al., 2013; Nolte et al., 2008; Melkonyan and Wagner, 2013). Over eastern China, the surface ozone concentration and possibility of severe ozone pollution may both increase in the future (Wang et al., 2013).

However, previous studies mainly focused on observational analyses of several synoptic processes, rather than long-term climate diagnostics, because of the lack of long-term surface O_3 observations. The goal of this study is to examine the large-scale atmospheric circulations associated with the interannual variation of summer surface O_3 pollution in North China based on long-term meteorological observations. The role of May Arctic sea ice, as a preceding and effective driver, were also analyzed. The outcomes of our research may provide a basis for understanding the interannual variation of O_3 pollution and its seasonal-to-interannual prediction.

2 Data and Method

The hourly O_3 concentration data from 2014 to 2017 in China were provided by the Ministry of Environmental Protection of China. The hourly O_3 concentration data from 2006–2017 at the Shangdianzi station (SDZ: located at 40°39'N, 117°07'E and 293.3 m high), one of the three regional background air-monitoring stations in China, were collected and controlled by the National Meteorological Information Center, China Meteorological Administration. According to the Technical Regulation on Ambient Air Quality Index (the Ministry of Environmental Protection of China, 2012), the maximum daily average 8 h concentration of ozone (MDA8) was calculated to represent the daily O_3 conditions. The monthly sea ice concentrations (1 °×1 °) were downloaded from the Met Office Hadley Center (Rayner et al. 2003), which are widely used in sea ice-related

Atmos. Chem. Phys. Discuss., https://doi.org/10.5194/acp-2018-1127
Manuscript under review for journal Atmos. Chem. Phys.
Discussion started: 19 November 2018
© Author(s) 2018. CC BY 4.0 License.

analysis.

The 1 °×1 ° ERA-Interim data used here included the geopotential height (Z), zonal and meridional wind, relative humidity, vertical velocity, air temperature at different pressure levels, boundary layer height (BLH), surface air temperature (SAT) and wind, downward UV radiation, downward solar radiation, low and medium cloud cover and precipitation (Dee et al. 2011). The daily and monthly ERA-Interim data were analyzed in this study. Furthermore, the daily and monthly reanalysis datasets supported by the National Oceanic and Atmospheric Administration (NOAA) were also employed and denoted as NOAA data. The 2.5 °×2.5 ° geopotential height (Z), zonal and meridional wind, relative humidity, vertical velocity, air temperature at different pressure levels, SAT and wind, downward UV radiation, downward solar radiation, low and medium cloud cover were downloaded from the National Center for Environmental Prediction and the National Center for Atmospheric Research (Kalnay et al. 1996). The BLH from 1979 to 2014 in the NOAA data was derived from the NOAA-CIRES 20th Century Reanalysis version 2c (Giese et al., 2016). The daily precipitation data was from the CPC global analysis of the daily precipitation dataset (Chen et al., 2008). The calculation procedure for the Eurasia teleconnection pattern (EUTP) index was consistent with that of Wang et al. (2015).

$$\text{EUTP index} = [-1\times\overline{\text{H500}}_{(70-80°N,60-90°E)} + 2\times\overline{\text{H500}}_{(45-55°N,90-110°E)} - 1\times\overline{\text{H500}}_{(35-45°N,120-140°E)}]/4$$

where H500 represents the geopotential height at 500 hPa, and overbars denote the area average.

3 Summer ozone pollution and associated weather conditions

Due to increased surface O_3 pollution in China, the number of O_3 measurement stations has dramatically increased since 2014 (Figure S1 a, c, e, g). During 2006–2014, O_3 concentrations were only observed in the most developed regions in China, i.e., the Beijing-Tianjin-Hebei area, the Yangtze River Delta, and the Pearl River Delta. Since 2015, O_3 concentrations have been measured in most areas in eastern China. O_3 concentrations in the high-mid latitudes were higher than those in the lower latitudes, which appeared to be bordered by the Yangtze River. The O_3 concentrations in North China were rather high in 2014; the summer mean maximum daily average 8 h concentration of ozone (MDA8) in North China was higher than 120 μg/m³. Since that time, the O_3 polluted region has expanded approximately yearly. In 2017, the areas with summer mean MDA8 > 120 μg/m³ were visibly enlarged. In North China, the summer mean MDA8 observations were larger than 150 μg/m³, and the maximum MDA8 was almost higher than 265 μg/m³ (i.e., the threshold of severe surface O_3 pollution). South of the Yangtze River, the O_3 concentrations were distinctly lower and decreased progressively towards the Pearl River Delta.

The time span of O_3 observations limited the possibility of determining the role of climate variability in the interannual O_3

© Author(s) 2018. CC BY 4.0 License.

variations in North China. Thus, we examined the representativeness of the O_3 measurements at Shangdianzi station (SDZ: one of the three regional background air-monitoring stations in China), with observations from 2006–2017. The correlation coefficients between SDZ MDA8 and the observed MDA8 at the other sites were calculated and are shown in Figure S1 (b, d, f, h). Similar to the O_3 concentrations, these correlation coefficients were also oppositely distributed south and north of 30oN. The SDZ MDA8 significantly covaried with the MDA8 in the north of China., especially in North China. The variation of summer SDZ MDA8 is presented in Figure S2. The diurnal difference in MDA8 was large, which contradicts the quasi-constant emission of ozone precursors. Therefore, the impacts of meteorological conditions were significant. According to the Technical Regulation on Ambient Air Quality Index in China (The Ministry of Environmental Protect of China, 2012), the thresholds of moderate surface O_3 pollution (MOP) and nonsurface O_3 pollution (NOP) are 215 μg/m³ and 100 μg/m³, respectively. During the years 2007–2017, there were 126 NOP days and 155 MOP days. The maximum number of MOP days was 26 days in 2015, and the mean number of MOP days was 14 days (Figure S3). The interannual variation in MOP (NOP) days was significant, without an obvious long-term trend.

The meteorological conditions were composited for the MOP and NOP days (Figure 1). The local and surrounding weather conditions were significantly different. The anomalous southerlies, higher boundary layer height (BLH), less rainfall, warmer surface air temperature, and cooler temperature in the high troposphere favored surface O_3 pollution and vice versa. Anomalous southerlies from the Yangtze River transported O_3 precursors (that were discharged in the economically developed Yangtze River Delta) and superposed them with the local high emissions in North China (Figure 1a). When the anomalous winds reversed, i.e., northerlies, the O_3 precursors in North China was dispersed, and the surface O_3 concentration was reduced (Figure 1b). The correlation coefficient between the SDZ O_3 concentration and the area-averaged meridional wind at 10 m (35–50oN, 110–122.5oN, denoted as V10mI) was 0.39, exceeding the 99% confidence level. The moisture environment (i.e., high relative humidity) and cloudy skies were essential conditions for precipitation, which weakened the photochemical reaction by influencing exposure to ultraviolet rays. In addition, precipitation was also an important indicator of the wet removal efficiency (Figure 1f). In summer, a day without rain represents efficient solar radiation, in favor of the occurrence of surface O_3 pollution (Figure 1e). The correlation coefficient between the area-averaged precipitation (37.5–42.5 ℅N, 112–127.5 ℅N, denoted as PI) and the SDZ O_3 concentration was –0.35 (above the 99% confidence level), indicating that sufficient precipitation was connected with more NOP days.

In contrast, the high temperature near the surface enhanced the photochemical reaction and resulted in a higher surface O_3 concentration (Figure 1 g). The sky without clouds not only provided strong solar radiation (i.e., warmer surface air temperature) but also resulted in weak absorption of long-wave radiation in the upper air (i.e., cooler temperature at 200 hPa). The correlation coefficient between the area-averaged difference in the temperature at the surface and 200 hPa (surface air temperature minus temperature at 200 hPa, 37.5–47.5 ℅N, 110–122.5 ℅N, denoted as DTI) and the SDZ O_3 concentration was

© Author(s) 2018. CC BY 4.0 License.

0.49. Furthermore, due to the strengthening of solar radiation, the near-surface turbulence was enhanced, and the boundary layer was lifted (Figure 1c). The downwash of atmospheric ozone from the upper air enlarged the surface O_3 concentration (An et al., 2009). The correlation coefficient between the SDZ O_3 concentration and the area-averaged BLH (37.5–47.5 ℃N, 112.5–120 ℃N, denoted as BI) was 0.40. Therefore, the anomalous southerlies, high surface temperature, above average BLH, and sunny skies were favorable environments for severe surface O_3 pollution. To confirm the robustness of the link between meteorological conditions and the MOP and NOP days over North China, the above composite analysis was repeated with NOAA reanalysis data, and identical results were obtained (Figures S4,5).

To assess the interannual variation of surface O_3 pollution and its relationship with climate variability (Cai et al., 2017), we tried to fit an O_3 weather index (OWI) based on long-term meteorological observations. Here, we defined the OWI as OWI=normalized V10mI+normalized BI–normalized PI+normalized DTI. For comparison, the multiple regression equation was built between the MDA8 and associated weather indices (Figure S6). Our analysis indicated that the observed MDA8 was well fit by the multiple regression equation (Figure S6). The correlation coefficient was 0.61 between the fit and daily measured MDA8 during 2007–2017 (i.e., 92 days × 11 years). In contrast, the correlation coefficient between the observed MDA8 and daily OWI was also 0.61 for the 11 year period. Thus, the OWI was easily constructed by accumulating the normalized weather index and was selected to represent the variation in surface O_3 pollution. A total of 90.3% of the MOP events were in the range of OWI > 0, and correspondingly, 90.5% of the NOP events were linked with OWI < 0 (Figure 2). The correlation coefficients between the OWI and observed MDA8 at the other sites were calculated (Figure S7). The significantly positive correlations were distributed in North China. Thus, it is reasonable to analyze the variation in surface O_3 pollution in North China using the OWI, which also extends the study period to the historical period before 2007 and the projected future.

4 Impacts of EUTP on the interannual variation of surface ozone

After 1979, the quality of the reanalysis data was improved to support studies of climate variability and change. Here, the daily OWI was calculated with both ERA-Interim and NOAA reanalysis data, and the monthly mean OWI was computed. During 2007–2017, the constructed JJA mean OWI varied similarly with the observed MDA8 and captured the extremes (Figure 3). In the above composite analysis and OWI construction processes, the range of the data used was 2007–2017; thus, the datasets in 2006 were independently verified samples. The JJA mean OWI in 2006 successfully reflected the variation in observed MDA8; even the MDA8 in 2006 was a staged minimum. Derived from two different reanalysis datasets, the OWI-ERA and OWI-NOAA varied consistently, confirming the robustness of the monthly OWI. In the following study, the monthly OWI from ERA-interim data and associated physical mechanisms were analyzed. Before the mid-1990s, the OWI was below zero, with a slightly decreasing trend and insignificant interannual variation. Since then, the OWI has significantly increased; furthermore, the intensity of interannual variation has strengthened. The emissions of O_3 precursors increased persistently and

© Author(s) 2018. CC BY 4.0 License.

linearly due to the steady economic development in China. We speculated that the strong interannual variation in surface O_3 pollution was significantly related to climate variability. Thus, the impacts of the large-scale atmospheric circulations were analyzed.

The atmospheric circulation associated with summer mean OWI, indicated by the correlation coefficients, are displayed in Figure 4–5. In the mid-upper troposphere, cyclonic and anticyclonic anomalies were alternately distributed over the north-central Siberian Plateau (–), North China and Mongolia (+), and the Yellow Sea and Japan Sea (–) (Figure 4a). These three atmospheric centers, propagated from the polar region to the mid-latitudes, appeared to be the EUTP. This Rossby wave-like train, i.e., the EUTP, could also be recognized in the surface air temperature. The correlation coefficient between the EUTP index and OWI was 0.44 (after detrending and above the 99% confidence level), indicating that the strengthening of the EUTP positive phase contributed to the severe surface O_3 pollution in North China. The EUTP is considered to be the main reason for the variability of the severe drought in North China, i.e., resulting in hot and dry climate extremes (Wang and He, 2015). To a certain extent, the severe drought environment promoted the formation of surface ozone. After 2007, the EUTP index and the observational SDZ MDA8 synchronously changed (Figure S8). More than 80% of the SDZ MDA8 anomalies showed the same mathematical sign as the anomalous EUTP index. Furthermore, the intensified EUTP anomalies (i.e., the |EUTP index| > 0.8 × its standard deviation) always induced homodromous surface ozone pollution.

Under barotropic anticyclonic circulation over North China, i.e., one of the active centers of the positive EUTP, the significant descending air flows indicated efficient adiabatic heating (resulting in high temperatures near the surface) and dry air (i.e., less cloud cover) below 300 hPa. Furthermore, over North China, the air temperature (relative humidity) anomalies were negative (positive) at 200 hPa but positive (negative) below 300 hPa (Figure 4c). The barotropic anticyclonic circulation associated with surface ozone pollution (Figure 4b) was similar to the positive EUTP (Figure 4c) and led to sunny days, i.e., hot temperatures (Figure 4a), strong downwards solar radiation and UV radiation (Figure 5c–d), less low and medium cloud cover (Figure 5d), and dry conditions (Figure 5b–c). Without the cover of low and medium clouds, the short wave solar radiation, especially the UV radiation, penetrated straight to the land surface. The photochemical reaction of the O_3 precursor was enhanced, generating more O_3 near the surface. The dry atmosphere near the surface, i.e., less precipitation and lower relative humidity, accelerated the photochemical reaction but restricted the wet clearing of the stocked O_3 in the atmosphere. A higher BLH (Figure 5b), resulting from the strengthening of solar radiation, facilitated the downward transportation of O_3 from aloft. Near the surface, the western part of these anticyclonic anomalies manifested as significant southerlies (Figure 5a), which transported the O_3 precursors from the economically developed Yangtze River Delta. The extraneous O_3 precursor, superposed with local emissions, supported a harsh and efficient photochemical reaction of O_3. To confirm the robustness of the atmospheric circulation and associated physical mechanisms, the above analysis was repeated with the NOAA data, and identical results were obtained (Figure S9–S10).

© Author(s) 2018. CC BY 4.0 License.

5 Roles of the Arctic sea ice

The positive EUTP enhanced the local anticyclonic circulation over North China and facilitated the processes leading to the formation of surface ozone. The EUTP originated from the Arctic region; thus, the role of Arctic sea ice on the OWI was also considered in this study. The interannual variation of OWI was significantly correlated with May sea ice conditions to the north of Eurasia, especially near the Gakkel Ridge, the Canada Basin and the Beaufort Sea (Figure 6a). The area-averaged (green boxes in Figure 6a) sea ice in May was calculated as the SI index, whose linear correlation coefficient with JJA OWI was 0.67 (after detrending) from 1979 to 2017. During 2007–2017, 73% of the May SI anomalies may be followed by observational SDZ MDA8 anomalies with the same mathematical sign (Figure 6b). Furthermore, the linear and nonlinear relationships were both introduced using the generalized additive model (Figure S11), and the contribution of May sea ice to the interannual variability of OWI was approximately 60%.

These positive sea ice anomalies could induce EUTP-like responses in the subsequent summer (Figure 6c). The excited atmospheric and thermal centers were located over the Central Siberian Plateau, North China and Mongolia, and the Yellow Sea. Similarly, the local meteorological responses, such as anomalous southerlies and less precipitation (Figure 6d), less cloud and strong solar radiation (Figure 6e) were also closely connected with the positive sea ice anomalies in May. Thus, the preceding May sea ice positively modulated the EUTP, and then, this Rossby wave train transported the impacts from the polar region and strengthened the anti-cyclonic anomalies over North China. Finally, suitable meteorological conditions, including hot-dry air, anomalous southerlies and intense sunshine, were induced to intensify the photochemical production of surface ozone pollution. To confirm the roles of Arctic sea ice and associated physical mechanisms, the above analysis was repeated with the NOAA data, and identical results were obtained (Figure S12).

6 Conclusions and discussions

Recently, the summer surface O_3 concentrations and the number of O_3 observation stations have steadily increased. Spatially, the O_3 concentrations in North China were substantially higher than those in South China. To reveal the climatic driver and improve the potential of seasonal prediction of summer surface O_3 pollution in North China, a daily OWI (i.e., surface O_3 weather index) was constructed based on long-term meteorological observations. The robustness of this index (i.e., OWI) was verified by the ERA-Interim and NOAA reanalysis datasets and surface O_3 measurements. May Arctic sea ice was found to be a preceding and efficient climatic driver. In the historical period, variation in Arctic sea ice can explain approximately 60% of the interannual variability of the summer surface O_3 pollution in North China. Currently, the Arctic region has been warming approximately twice as much as the global average (Huang et al., 2017; Zhou, 2017), indicating accelerated change in the sea ice. Thus, understanding the role of Arctic sea ice may contribute to the seasonal forecasting of O_3 pollution.

© Author(s) 2018. CC BY 4.0 License.

The EUTP acted as an atmospheric bridge to link May Arctic sea ice and the summer surface O_3 pollution in North China. The accumulated sea ice in May could induce or enhance the positive EUTP phase. The anticyclonic circulation over North China, i.e., one of the active centers of the EUTP, was connected with high surface temperature, strong downward solar radiation, less low and medium cloud cover, and drought over North China. Under such local meteorological conditions, the photochemical reaction to produce surface O_3 was accelerated. Generally, these anticyclonic anomalies over North China were barotropic and could persist for a long time; thus, the processes that produce surface O_3 were continuous to achieve a fairly high concentration. The connections revealed in this study were based on long-term meteorological measurements and thus provide possibilities for the seasonal to interannual prediction of O_3 pollution. The seasonal outlook helps to determine whether extra stringent control measures on regional O_3 precursor emissions are needed to counteract the effect of climate variability.

Author contribution

Yin Z. C. and Wang H. J. designed the research. Yin Z. C., Li Y. Y. and Ma X. H. performed research. Yin Z. C. and Zhang X. Y. analysed data. Yin Z. C. prepared the manuscript with contributions from all co-authors.

The authors declare no conflict of interest.

Acknowledgments

This research was supported by the National Key Research and Development Plan (2016YFA0600703), the National Natural Science Foundation of China (91744311 and 41705058), the CAS–PKU Partnership Program, and the Jiangsu innovation & entrepreneurship team.

© Author(s) 2018. CC BY 4.0 License.

Reference

An, J. L., Wang, Y. S., and Sun, Y. Assessment of ozone variations and meteorological effects in Beijing, Ecology and Environmental Sciences, 18(3), 944–951,2009 (in Chinese).

Barnes, E. A. and Fiore, A. M.: Surface ozone variability and the jet position: Implications for projecting future air quality, Geophys. Res. Lett., 40, 2839–2844, 2013.

Cai, W. J., Li, K., Liao, H., Wang, H. J., and Wu, L. X.: Weather Conditions Conducive to Beijing Severe Haze More Frequent under Climate Change, Nature Climate Change, https://doi.org/10.1038/nclimate3249, 2017.

Chen, M., Xie, P., and CPC Precipitation Working Group.: CPC Unified Gauge-based Analysis of Global Daily Precipiation, Western Pacific Geophysics Meeting, Cairns, Australia, 29 July - 1 August, 2008.

Chen, Y., Ebenstein, A., Greenstone, M., and Li, H.: Evidence on the impact of sustained exposure to air pollution on life expectancy from China's Huai River policy, Atmospheric Chemistry and Physics, 110, 12936–12941, 2013.

Christoudias, T., Pozzer, A., and Lelieveld, J.: Influence of the North Atlantic Oscillation on air pollution transport, Atmos. Chem. Phys., 12, 869–877, https://doi.org/10.5194/acp-12-869-2012, 2012.

Dee, D. P., Uppala, S. M., Simmons, A. J., Berrisford, P., Poli, P., Kobayashi, S., Andrae, U., Balmaseda, M. A., Balsamo, G., Bauer, P., Bechtold, P., and Beljaars, A. C. M.: The ERA-Interim reanalysis: configuration and performance of the data assimilation system, Q. J. Roy. Meteor. Soc., 137, 553–597, https://doi.org/10.1002/qj.828, 2011.

Doherty, R. M., Wild, O., and Shindell, D. T., et al.: Impacts of climate change on surface ozone and intercontinental ozone pollution: A multi-model study, Journal of Geophysical Research Atmospheres, 118(9), 3744–3763, 2013.

Giese, B.S., Seidel, H.F., Compo, G.P., and Sardeshmukh, P.D.: An ensemble of ocean reanalyses for 1815-2013 with sparse observational input, J. Geophys. Res. Oceans, 121, 6891–6910, https://doi.org/10.1002/2016JC012079, 2016.

Huang, X. T., Diao, Y. N., and Luo, D. H.: Amplified winter Arctic tropospheric warming and its link to atmospheric circulation changes, Atmos. Oceanic Sci. Lett., 10(6), 435–445, https://doi.org/ 10.1080/16742834.2017.1394159, 2017.

Kalnay, E., Kanamitsu, M., Kistler, R., Collins, W., Deaven, D., Gandin, L., Iredell, M., Saha, S., White, G., Woollen, J., Zhu, Y., Leetmaa, A., Reynolds, R., Chelliah, M., Ebisuzaki, W., Higgins, W., Janowiak, J., Mo, K. C., Ropelewski, C., Wang, J., Jenne, R., and Joseph, D.: The NCEP/NCAR 40-year reanalysis project, Bull. Am. Meteorol. Soc., 77, 437–471, https://doi.org/10.1175/1520-0477(1996)077<0437: TNYRP>2.0. CO;2, 1996.

Li, R. X., and Sun, J. Q.: Interdecadal variability of the large-scale extreme hot event frequency over the middle and lower reaches of the Yangtze River basin and its related atmospheric patterns, Atmos. Oceanic Sci. Lett., 11(1), 63–70, https://doi.org/ 10.1080/16742834.2017.1335580, 2018.

Liu, R. J., and Liao, H.: Assessment of aerosol effective radiative forcing and surface air temperature response over eastern China in CMIP5 models, Atmos. Oceanic Sci. Lett., 10(3), 228–234, https://doi.org/10.1080/16742834.2017.1301188, 2017.

© Author(s) 2018. CC BY 4.0 License.

Lin, M., Fiore, A. M., Horowitz, L. W., Langford, A. O., Oltmans, S. J., Tarasick, D., and Eieder, H.: Climate variability modulates western us ozone air quality in spring via deep stratospheric intrusions, Nature Communications, 6, 7105, 2015.

Lin, M. Y., Horowitz, L. W., Oltmans, S. J., Fiore, A. M., and Fan, S. M.: Tropospheric ozone trends at Mauna Loa Observatory tied to decadal climate variability, Nature Geoscience, 7, 136–143, 2014.

Ma, Z., Xu, J., Quan, W., Zhang, Z., Lin, W., and Xu X.: Significant increase of surface ozone at a rural site, north of eastern China, Atmospheric Chemistry and Physics, 16(6), 3969–3977, 2016.

Melkonyan, A., and Wagner, P.: Ozone and its projection in regard to climate change, Atmospheric Environment, 67(2), 287-295, 2013.

Nolte, C. G., Gillil, A. B., and Hogrefe, C., et al.: Linking global to regional models to assess future climate impacts on surface ozone levels in the United States, Journal of Geophysical Research: Atmospheres (1984–2012), 762–770, 2008.

Pausata, F. S. R., Pozzoli, L., Vignati, E., and Dentener, F. J.: North Atlantic Oscillation and tropospheric ozone variability in Europe: model analysis and measurements intercomparison, Atmos. Chem. Phys., 12, 6357–6376, https://doi.org/10.5194/acp-12-6357-2012, 2012.

Pu, X., Wang, T. J., and Huang, X., et al.: Enhanced surface ozone during the heat wave of 2013 in Yangtze River Delta region, China, Science of the Total Environment, 603–604, 807–816, 2017.

Rayner, N. A., D. E. Parker, E. B. Horton, C. K. Folland, L. V. Alexander, D. P. Rowell, E. C. Kent, and A. Kaplan.: Global analyses of sea surface temperature, sea ice, and night marine air temperature since the late nineteenth century. J. Geophys. Res., 108, 4407, doi:10.1029/2002JD002670, 2003.

Shi, C., Wang, S., Liu, R., Zhou, R., Li, D., and Wang, W., et al.: A study of aerosol optical properties during ozone pollution episodes in 2013 over Shanghai, China. Atmos. Res., 153, 235–249, 2015.

Tang, B. Y., Xin, J. Y., Gao, W. K., Shao, P., Su, H. J., Wen, T. X., Song, T., Fan, G. Z., Wang, S. G., and Wang, Y. S.: Characteristics of complex air pollution in typical cities of North China, Atmos. Oceanic Sci. Lett., 11(1), 29–36, https://doi.org/10.1080/16742834.2018.1394158, 2018.

The environmental statistics unit of stat-center in Perking University. Air quality Assessment Report (5): the assessments of the regional pollutions in “2+31” cities during 2013–2017, http://songxichen.gsm.pku.edu.cn/index.php/Research/#tab_34, 2018.

The Ministry of Environmental Protect of China: Technical Regulation on Ambient Air Quality Index, 1pp, 2012.

Tong, L., Zhang, H. L., Yu, J., He, M. M., Xu N. B., Zhang, J. J., Qian F. Z., Feng J. Y., and Xiao, H.: Characteristics of surface ozone and nitrogen oxides at urban, suburban and rural sites in Ningbo, China, Atmospheric Research, 187: 57–68, 2017.

Wang, H. J.: On assessing haze attribution and control measures in China, Atmospheric and Oceanic Science Letters, 11:2, 120-122, DOI: 10.1080/16742834.2018.1409067, 2018.

© Author(s) 2018. CC BY 4.0 License.

Wang, H. J., and He, S. P.: The North China/Northeastern Asia Severe Summer Drought in 2014, Journal of Climate, 28(17), 6667–6681, 2015.

Wang, T.: Ozone pollution in China: A review of concentrations, meteorological influences, chemical precursors, and effects, Science of The Total Environment, 575: 1582-1596, 2017.

Wang, T., Ding, A., Gao, J., and Wu, W. S.: Strong ozone production in urban plumes from Beijing, China, Geophys. Res. Lett., 33(21), 320–337, 2006.

Wang, Y. X., Shen, L. L., Wu, S. L., Mlckley, L., He, J. W., and Hao, J. M.: Sensitivity of surface ozone over China to 2000–2050 global changes of climate and emissions, Atmospheric Environment, 75, 372–382, 2013.

Watts, N., Amann, M., Ayeb-Karlsson, S., et al.: The Lancet Countdown on health and climate change: From 25 years of inaction to a global transformation for public health, Lancet, 391, 10–16, 2018.

Yan, Y., Pozzer, A., Ojha, N., Lin, J., and Lelieveld, J.: Analysis of european ozone trends in the period 1995-2014, Atmospheric Chemistry and Physics, 18(8), 5589-5605, 2017.

Yang, Y., Liao, H., and Li, J.: Impacts of the East Asian summer monsoon on interannual variations of summertime surface-layer ozone concentrations over China, Atmos. Chem. Phys., 14, 6867–6879, 2014.

Yin, Z. C., Wang, H. J., and Guo, W. L.: Climatic change features of fog and haze in winter over North China and Huang-Huai Area, SCIENCE CHINA Earth Sciences, 58(8), 1370–1376, 2015.

Zhao, Z. J., and Wang, Y. X.: Influence of the West Pacific subtropical high on surface ozone daily variability in summertime over eastern China, Atmospheric Environment, 180, 197–204, 2017.

Zhou, W.: Impact of Arctic amplification on East Asian winter climate. Atmos. Oceanic Sci. Lett., 10(5), 385-388, doi: 10.1080/16742834.2017.1350093, 2017.

© Author(s) 2018. CC BY 4.0 License.

Table and Figures captions

Figure 1. Composite of the meteorological conditions associated with different O_3 events during 2007–2017. Results for MOP (a, c, e, g) and NOP (b, d, f, h) events included (a–b) surface wind (arrow) and v-wind (shading), (c–d) BLH, (e–f) precipitation, (g–h) SAT, and temperature at 200 hPa. The black dots denote the composite results passed the 95% confidence level. The boxes represent the area used to calculate OWI. These composites were calculated using the ERA-Interim datasets.

Figure 2. The OWI for MOP (red) and NOP (blue) events during 2007–2017.

Figure 3. The variation in the JJA mean observed SDZ MDA8 (green) from 2006 to 2017, OWI calculated from ERA-interim datasets during 1979–2017 (blue) and OWI calculated from NOAA datasets (red) during 1979–2014.

Figure 4. The associated atmospheric circulation. (a) The correlation coefficients between the JJA mean OWI and surface air temperature (shading), wind (arrow) at 200 hPa and geopotential height at 500 hPa (contour) from 1979 to 2017. The black dots indicate that the CC with surface air temperature was above the 95% confidence level. The cross-section (110 °–125 °E mean) correlation coefficients between JJA mean OWI (a), EUTP index (b) and relative humidity (shading), temperature (contour), wind (arrow, vertical speed multiplied by 100) from 1979 to 2017. The black dots indicate that the CC with relative humidity exceeded the 95% confidence level (t test). The data used here are ERA-Interim datasets.

Figure 5. The associated meteorological conditions. (a) The correlation coefficients between the JJA mean OWI and v wind at 10 m (shading), surface wind (arrow), (b) relative humidity near the surface (shading), boundary layer height (contour), (c) precipitation (shading), downward UV radiation at the surface (contour), (d) downward solar radiation at the surface (shading), sum of low and medium cloud cover (contour) from 1979 to 2017. The black dots indicate that the CC with temperature was above the 95% confidence level. The contours plotted in panel (b–d) exceeded the 95% confidence level. The data used here are ERA-Interim datasets.

Figure 6. The role of the Arctic sea ice. (a) The correlation coefficients between the JJA mean OWI and May sea ice, (b) The variation of the May SI index (red bar, area-averaged sea ice of the green boxes in panel a), JJA mean EUTP index (blue bar) and JJA mean observational SDZ MDA8 (black bar) from 2007 to 2017. (c) The correlation coefficients between the May SI index and surface air temperature (shading), geopotential height at 500 hPa (contour) from 1979 to 2017. The black dots indicate that the CC with surface air temperature was above the 95% confidence level. (d) The correlation coefficients between the May SI index and precipitation (shading), surface wind (arrow), (e) downward UV radiation at the surface (shading) and sum of low and medium cloud cover (contour) from 1979 to 2017. The black dots indicate that the shading CC with precipitation (d) and downward UV radiation (e) was above the 95% confidence level. The data used here are ERA-Interim datasets.

Atmos. Chem. Phys. Discuss., https://doi.org/10.5194/acp-2018-1127
Manuscript under review for journal Atmos. Chem. Phys.
Discussion started: 19 November 2018
© Author(s) 2018. CC BY 4.0 License.

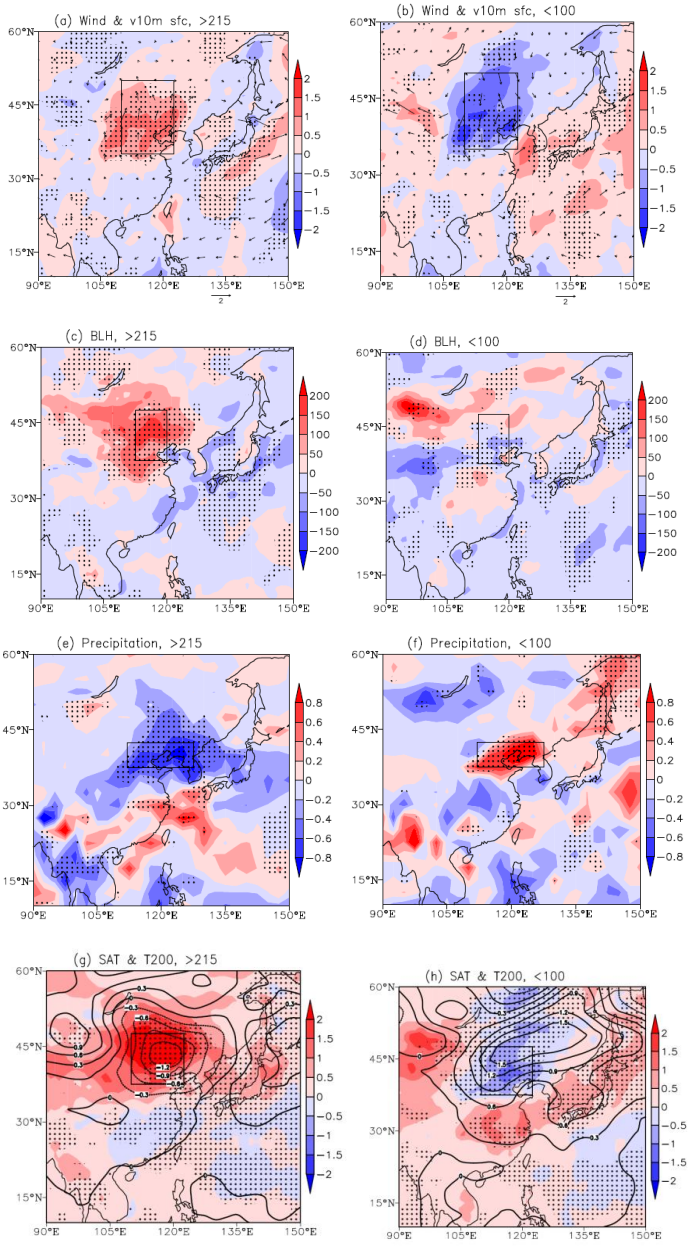

365 **Figure 1. Composite of the meteorological conditions associated with different O_3 events during 2007–2017. Results for MOP (a, c, e, g) and NOP (b, d, f, h) events included (a–b) surface wind (arrow) and v-wind (shading), (c–d) BLH, (e–f) precipitation, (g–h) SAT, and temperature at 200 hPa. The black dots denote the composite results passed the 95% confidence level. The boxes represent the area used to calculate OWI. These composites were calculated using the ERA-Interim datasets.**

Atmos. Chem. Phys. Discuss., https://doi.org/10.5194/acp-2018-1127
Manuscript under review for journal Atmos. Chem. Phys.
Discussion started: 19 November 2018
© Author(s) 2018. CC BY 4.0 License.

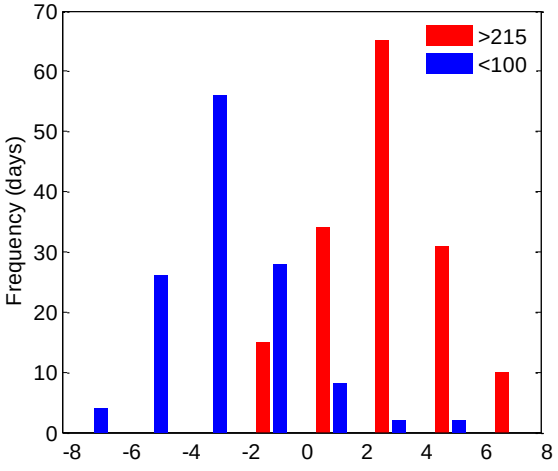

370 **Figure 2. The OWI for MOP (red) and NOP (blue) events during 2007–2017.**

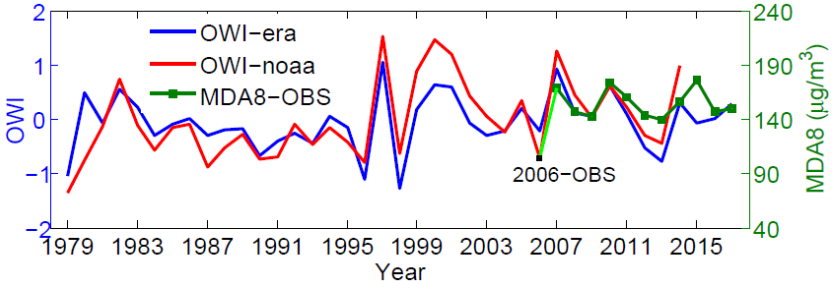

Figure 3. The variation in the JJA mean observed SDZ MDA8 (green) from 2006 to 2017, OWI calculated from ERA-interim datasets during 1979–2017 (blue) and OWI calculated from NOAA datasets (red) during 1979–2014.

Atmos. Chem. Phys. Discuss., https://doi.org/10.5194/acp-2018-1127
Manuscript under review for journal Atmos. Chem. Phys.
Discussion started: 19 November 2018
© Author(s) 2018. CC BY 4.0 License.

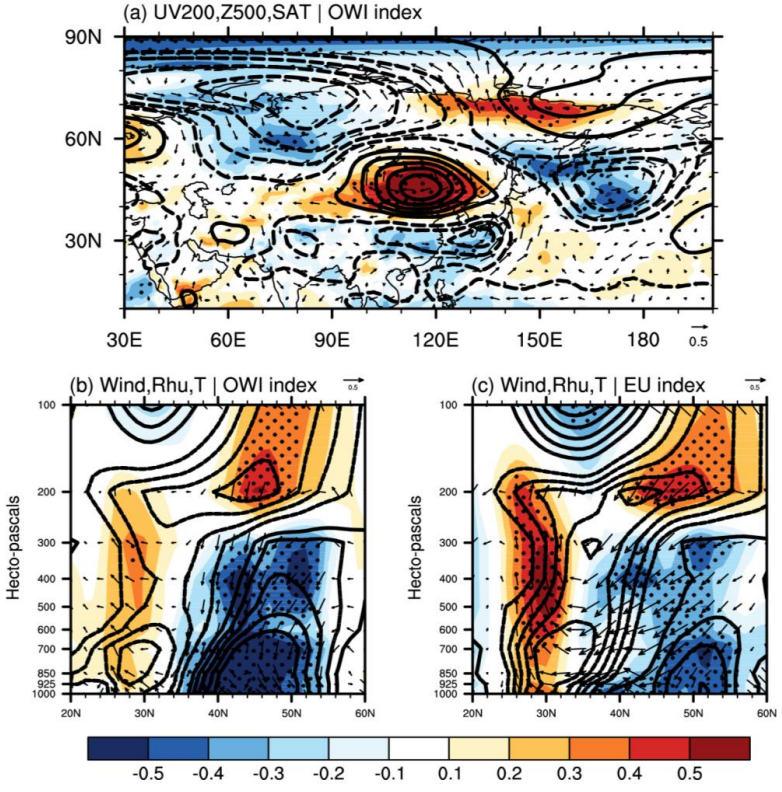

Figure 4. The associated atmospheric circulation. (a) The correlation coefficients between the JJA mean OWI and surface air temperature (shading), wind (arrow) at 200 hPa and geopotential height at 500 hPa (contour) from 1979 to 2017. The black dots indicate that the CC with surface air temperature was above the 95% confidence level. The cross-section (110°–125°E mean) correlation coefficients between JJA mean OWI (a), EUTP index (b) and relative humidity (shading), temperature (contour), wind (arrow, vertical speed multiplied by 100) from 1979 to 2017. The black dots indicate that the CC with relative humidity exceeded the 95% confidence level (t test). The data used here are ERA-Interim datasets.

Atmos. Chem. Phys. Discuss., https://doi.org/10.5194/acp-2018-1127
Manuscript under review for journal Atmos. Chem. Phys.
Discussion started: 19 November 2018
© Author(s) 2018. CC BY 4.0 License.

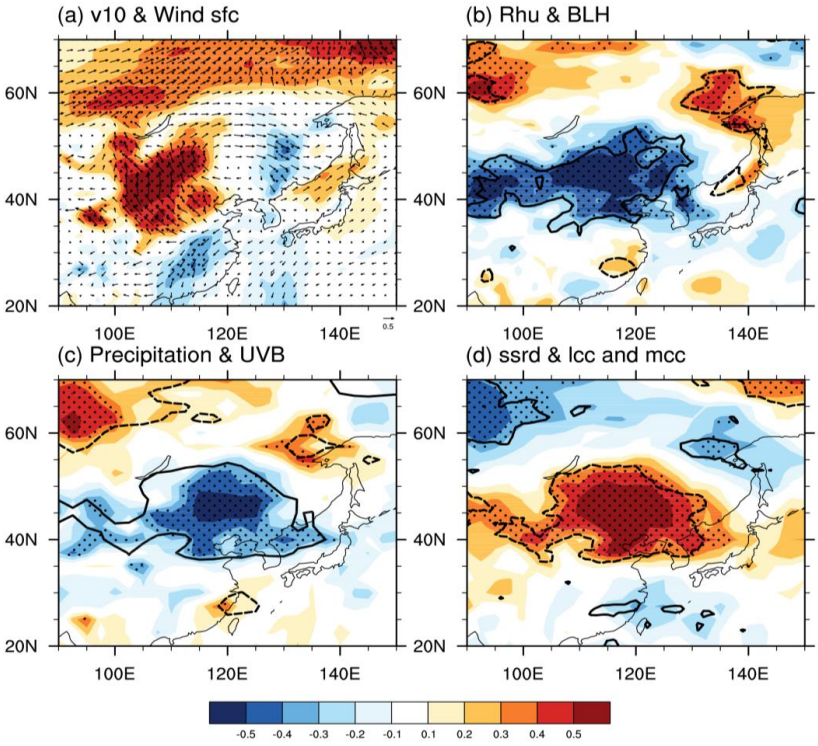

Figure 5. The associated meteorological conditions. (a) The correlation coefficients between the JJA mean OWI and v wind at 10 m (shading), surface wind (arrow), (b) relative humidity near the surface (shading), boundary layer height (contour), (c) precipitation (shading), downward UV radiation at the surface (contour), (d) downward solar radiation at the surface (shading), sum of low and medium cloud cover (contour) from 1979 to 2017. The black dots indicate that the CC with temperature was above the 95% confidence level. The contours plotted in panel (b–d) exceeded the 95% confidence level. The data used here are ERA-Interim datasets.

Atmos. Chem. Phys. Discuss., https://doi.org/10.5194/acp-2018-1127
Manuscript under review for journal Atmos. Chem. Phys.
Discussion started: 19 November 2018
© Author(s) 2018. CC BY 4.0 License.

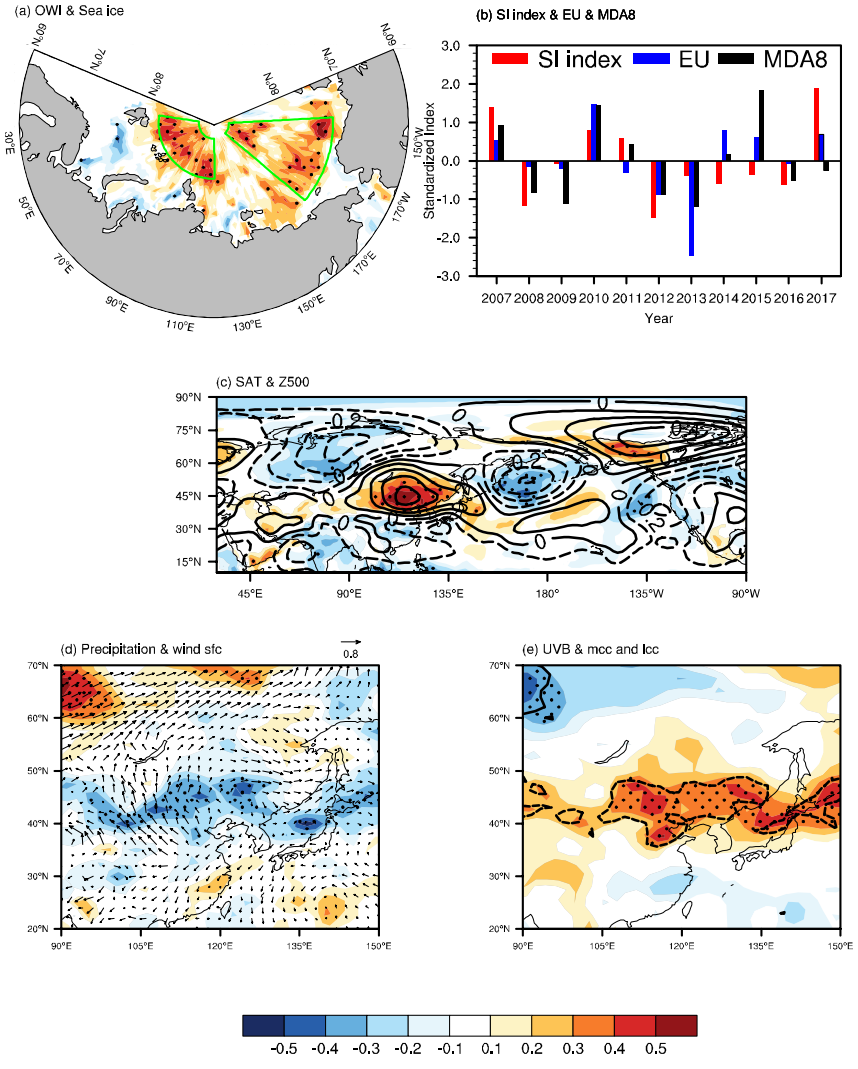

Figure 6. The role of the Arctic sea ice. (a) The correlation coefficients between the JJA mean OWI and May sea ice, (b) The variation of the May SI index (red bar, area-averaged sea ice of the green boxes in panel a), JJA mean EUTP index (blue bar) and JJA mean observational SDZ MDA8 (black bar) from 2007 to 2017. (c) The correlation coefficients between the May SI index and surface air temperature (shading), geopotential height at 500 hPa (contour) from 1979 to 2017. The black dots indicate that the CC with surface air temperature was above the 95% confidence level. (d) The correlation coefficients between the May SI index and precipitation (shading), surface wind (arrow), (e) downward UV radiation at the surface (shading) and sum of low and medium cloud cover (contour) from 1979 to 2017. The black dots indicate that the shading CC with precipitation (d) and downward UV radiation (e) was above the 95% confidence level. The data used here are ERA-Interim datasets.